https://doi.org/10.5194/egusphere-2026-145
Preprint. Discussion started: 5 February 2026

Tropical forest responses to climate extremes: an analysis using an individual-based demographic vegetation model

Mazen Nakad[1], Mahmoud Mbarak[2], Jihad Karaki[3], Tehreem Qureshi[4], Matteo Detto[5], Benjamin I. Cook[6], Marcos Longo[7,8], Géraldine Derroire[9], Xiangtao Xu[10], Jeremy Lichstein[11], Zong-Liang Yang[2], Pierre Gentine[12,13], and Ensheng Weng[4,6]

[1]Chemical Engineering Department, Lebanese American University, Byblos, Lebanon
[2]Jackson School of Geosciences, University of Texas at Austin, Austin, USA
[3]Department of Mechanical Engineering, Politecnico di Milano, Milan, Italy
[4]Center for Climate Systems Research, Columbia University, New York City, USA
[5]Department of Ecology and Evolutionary Biology, Princeton University, Princeton, USA
[6]NASA Goddard Institute for Space Studies, New York City, USA
[7]Climate and Ecosystem Sciences Division, Lawrence Berkeley National Laboratory, Berkeley, USA
[8]Divisão de Modelagem Numérica do Sistema Terrestre, Coordenação-Geral de Ciências da Terra, Instituto Nacional de Pesquisas Espaciais, São José dos Campos, Brazil
[9]AgroParisTech, CNRS, INRAE, Université des Antilles, Université de Guyane, Kourou, France
[10]Department of Ecology and Evolutionary Biology, Cornell University, Ithaca, USA
[11]Department of Biology, University of Florida, Gainesville, USA
[12]Department of Earth and Environmental Engineering, Columbia University, New York City, USA
[13]Center for Learning the Earth with Artificial Intelligence and Physics, Columbia University, New York City, USA

Correspondence: Mazen Nakad (mazen.nakad@lau.edu.lb)

Abstract. Tropical forests play a crucial role in the global carbon and water cycles, yet their response to the climate extremes remains uncertain. Here, an individual-based demographic vegetation model is used to investigate the effects of warming and drought on ecosystem dynamics across three neotropical sites that span a precipitation gradient. By explicitly resolving plant hydraulic constraints and demographic processes, the study provides a mechanistic understanding of forest responses to climate stressors. The results reveal that warming had the strongest impact on carbon assimilation in the wettest sites (Paracou and Barro Colorado Island). This reduction was primarily driven by a rising vapor pressure deficit, which induced hydraulic failure even in the absence of soil moisture depletion. In contrast, the driest site (Tapajos National Forest) exhibited the highest sensitivity to drought, driven by severe soil moisture depletion. The analysis also shows that the timescale of imposed stress matters: short daily hot-dry events led to weaker impacts due to partial recovery between pulses, whereas yearly-scale warming and drought produced much stronger, persistent reductions in productivity. These findings highlight the site-specific vulnerabilities of tropical forests to climate extremes, where VPD-induced hydraulic stress limits carbon assimilation under warming in moist sites, while soil moisture constraints dominate in drier ecosystems.

https://doi.org/10.5194/egusphere-2026-145
Preprint. Discussion started: 5 February 2026

1 Introduction

Tropical forests play a fundamental role in the global carbon and water cycles, storing approximately 55% of global forest above-ground carbon and contributing up to 35% of the terrestrial carbon sink (Pan et al., 2024; Malhi, 2010; Ciais et al., 2014). These ecosystems regulate regional and global climate by modulating atmospheric CO_2, driving evapotranspiration, and influencing precipitation patterns, thus serving as critical buffers against climate variability and as essential players in mitigating additional atmospheric accumulation of CO_2 (Bonan, 2008). However, despite their importance, significant uncertainties remain regarding how tropical forests respond to changes in climate, particularly altered precipitation regimes, increased temperatures, and intensifying drought events (Feng et al., 2018; Sullivan et al., 2024; Janssen et al., 2020). Recent research highlights that forest productivity trends vary across ecosystems, as regional climatic fluctuations, including drought severity and temperature extremes, can lead to contrasting responses, with some forests demonstrating resilience while others experience substantial declines in productivity and carbon sequestration (Hubau et al., 2020; Hogan et al., 2024; Flack-Prain et al., 2019; Von Buttlar et al., 2018).

Future climate projections indicate significant changes in tropical precipitation patterns, with some regions such as Central America and the Amazon expected to experience severe declines, while others remain uncertain (Seneviratne et al., 2021; Parsons, 2020). CMIP6 models project increases in both drought frequency and duration, potentially driving widespread shifts in forest structure and function (Cook et al., 2020; Ukkola et al., 2020). Although these models provide valuable insights into large-scale climate trends, they often lack the ecological resolution needed to predict how forests respond at the demographic level. As rainfall variability intensifies, traditionally wet forests may experience moisture stress, whereas drier forests may endure prolonged droughts. Such conditions impose physiological stress, disrupt carbon balance, and increase mortality rates (Hilker et al., 2014; Xu et al., 2024). These changes may reshape species composition, alter carbon cycling, and compromise the long-term resilience of tropical ecosystems (Brienen et al., 2015; Lin et al., 2025), yet the extent to which warming and drought differentially impact forest function remains unresolved (Bottino et al., 2024).

Two fundamental challenges remain in predicting how tropical forests will respond to future hydroclimatic change. First, water stress arises from the combined effects of reduced rainfall, which limits water supply, and increased vapor pressure deficit (VPD), which intensifies atmospheric water demand. Second, drought and warming intensification occur across multiple time scales—including daily and seasonal anomalies, annual deficits, and multi-year oscillations, each imposing distinct physiological and demographic pressures on forest ecosystems (Jiménez-Muñoz et al., 2016; Flach et al., 2021; Tschumi et al., 2022). Consequently, this study aims to answer the following questions: (i) How are tropical forest carbon fluxes and hydraulic stress altered when changes in water supply (rainfall) and atmospheric water demand (VPD) are imposed independently or jointly? (ii) How are forest productivity and long-term resilience influenced by the time scale at which drought and warming intensification occurs (daily, seasonal, annual, and ENSO-like cycles)?

Field experiments have provided critical insights into tropical forest responses to drought. For example, the drought experiment conducted by Rowland et al. (2015) in the Amazon demonstrated that hydraulic failure, rather than carbon starvation, is the primary driver of mortality during severe drought. However, such experiments are constrained in spatial scale and duration

https://doi.org/10.5194/egusphere-2026-145
Preprint. Discussion started: 5 February 2026

and cannot systematically explore the diversity of drought and warming scenarios anticipated under future climate change. Moreover, it is practically unfeasible to replicate multi-year climate variability such as ENSO in controlled field experiments, and field manipulations are rarely long enough to capture slow ecological processes such as species turnover or shifts in community composition. For these reasons, modeling approaches have become essential tools for investigating how tropical forests may respond under a broad range of future climate extremes.

Vegetation Demography Models (VDMs) provide crucial capabilities to simulate forest structure, vegetation dynamics, and competitive interactions under changing environmental conditions (Fisher et al., 2018; Koven et al., 2020; Martínez Cano et al., 2020; Weng et al., 2022; Shevliakova et al., 2024; Maréchaux et al., 2025; Schmitt et al., 2025). These models share core features, including explicit size-structured demography and height-structured light competition among cohorts, enabling controlled climatic perturbations and mechanistic exploration of ecosystem responses. This allows the investigation of scenarios that cannot be tested experimentally, such as intensified drought regimes, modified rainfall periodicity, or idealized ENSO events.

Despite advances in modeling, a process-based understanding of how tropical forests structurally and functionally adapt to climate extremes remains incomplete. For instance, Robbins et al. (2024) used a hydrodynamic vegetation model to predict that future climate conditions could double the likelihood of xylem embolism and mortality, while Koch and Kaplan (2022) evaluated tropical forest carbon sequestration potential under climate change. Although these studies provide valuable insights into plant hydraulics and ecosystem carbon dynamics, many existing models rely on empirical or phenomenological relationships and do not fully account for how size-structured competition, resource allocation strategies, and ecosystem fluxes evolve under warming and drought. Shifts in tropical forest functional composition under increasing drought and CO_2 levels have been attributed to trade-offs in plant hydraulic traits (Bauman et al., 2022; Rowland et al., 2015), emphasizing the need for models that explicitly resolve physiological dynamics. In particular, interactions between warming and drought remain poorly understood, as their effects on ecosystem fluxes, water-use strategies, and competitive dynamics are nonlinear and site-dependent.

To address these knowledge gaps, the Biome Ecological Strategy Simulator (BiomeE) (Weng et al., 2019, 2022) is used in this study. BiomeE simulates forest structure through coupled mechanistic processes of plant hydraulics, carbon allocation, and competition dynamics, and allows independent manipulation of rainfall, temperature, and VPD across multiple time scales. This modeling framework enables the exploration of complex climate extremes that cannot be imposed in field experiments. Given the critical role of plant hydraulics and stomatal function in mediating responses to water stress (Detto and Pacala, 2022), the integration of mechanistic modeling with site-specific climate scenarios provides a process-based assessment of tropical forest resilience and vulnerability under interacting warming and drought.

2 Materials and Methods

2.1 Demographic vegetation model

BiomeE is a process-based demographic vegetation model developed to simulate complex ecological dynamics within plant communities (Weng et al., 2019). It builds on the Geophysical Fluid Dynamics Laboratory's LM3-PPA model (Weng et al.,

https://doi.org/10.5194/egusphere-2026-145
Preprint. Discussion started: 5 February 2026

2015), sharing core features such as the representation of plant physiology, vegetation demography, resource competition, and the coupled cycles of carbon, nitrogen, and water in ecosystems (Weng et al., 2022). BiomeE incorporates a competitive, game-theoretic framework to model vegetation dynamics through optimal allocation strategies. This approach enables BiomeE to simulate competitive interactions for light, water, and nutrients under varying environmental conditions. Similar to other demographic vegetation models, it integrates individual-level physiological processes with community-level dynamics and accounts for trait diversity, hydraulic functioning, and resource allocation strategies, providing insights into how these factors shape vegetation structure and ecosystem function. A schematic diagram illustrating the model's vegetation, biogeochemical, and hydraulic processes is shown in Figure 1. In BiomeE, individual plants are the fundamental units of ecological interactions, undergoing physiological processes such as photosynthesis, respiration, growth, reproduction, and mortality. The model represents competitive interactions among plants for essential resources like light and soil nutrients (Farrior et al., 2013; Dybzinski et al., 2011).

Water availability is an important control on plant performance and ecosystem structure. BiomeE integrates a mechanistic plant hydraulic framework based on Xu et al. (2016), which governs water transport from the soil through the plant to the atmosphere. This model accounts for key hydraulic traits such as xylem conductivity, turgor loss point, and cavitation vulnerability, influencing stomatal conductance, photosynthesis, and plant water status under different environmental conditions. The plant hydraulic model simulates the soil-plant-atmosphere continuum, tracking water flow from the soil through the root system, stem, and leaves, ultimately to the atmosphere.

Soil moisture is represented by a simple bucket model, in which a single root-zone water store is forced by precipitation, evapotranspiration, and drainage; the resulting soil water content and potential provide the lower boundary condition for the hydraulic model. The plant hydraulic model incorporates key processes such as water uptake, sap flow, cavitation effects, and recovery, capturing both the diurnal and seasonal dynamics of plant water status. By linking hydraulic function with photosynthetic capacity, the model provides a robust representation of plant responses to water stress and their impact on growth, carbon assimilation, and community dynamics.

Plants are grouped into cohorts and arranged into vertical canopy layers based on height and crown area, following the perfect plasticity approximation model (Strigul et al., 2008). Sunlight distribution among these layers is determined using Beer-Lambert's law, providing a simplified yet effective representation of light attenuation through the canopy. This approach allows for the simulation of light competition, particularly under varying canopy structures. Such effects could influence the sensitivity of modeled responses to drought stress, although the detailed hydraulic model integrated into BiomeE helps to mitigate these limitations by providing robust water dynamics representation.

The model captures vegetation structural dynamics, reflecting changes in cohort size distribution, density, and canopy structure over time. As plants grow, reproduce, and die, the overall canopy architecture and resource distribution evolve. BiomeE also integrates biogeochemical processes driven by both plants and soil microbes, ensuring a robust simulation of carbon and nitrogen flows between plant and soil pools, influenced by plant mortality and microbial decomposition. Cohorts, which are the primary units for physiological and demographic processes, undergo various changes in size and density due to the model's demographic processes. BiomeE simulates competition for light, soil resources, and water, community assembly, and

https://doi.org/10.5194/egusphere-2026-145
Preprint. Discussion started: 5 February 2026

vegetation structural dynamics through detailed cohort size and crown structure representation. These processes are organized hierarchically and operate at different time intervals: hourly for plant physiology, soil organic matter decomposition, and water dynamics; daily for growth and phenology; and annually for demography.

The environmental conditions at each site were used to initialize and run BiomeE. The model was run until equilibrium was reached, defined as a state where interannual variations in carbon and water fluxes, such as gross primary production and transpiration, and forest structure, such as leaf area index, fluctuated around a stable long-term mean with no consistent change over time. The spin-up period, during which the model adjusts to the meteorological boundary conditions, varied for each site depending on the specific meteorological data and model parameters. This period is crucial for ensuring that the model accurately reflects the long-term dynamics of the ecosystem. Once equilibrium was achieved, the model parameters were systematically altered to simulate various climate scenarios, including increased temperature, reduced precipitation, and combined warming and drought events. These modifications were designed to reflect potential future climate conditions and their impact on tropical forests.

For this study, BiomeE was configured with a single plant functional type (PFT), representing an evergreen broadleaf tropical tree, initialized from the model's default tropical PFT parameterization Weng et al. (2022) and refined using site-specific trait data from (Longo et al., 2018). Several core traits were held constant to maintain consistency, including its woody life-form, evergreen habit, C3 photosynthetic pathway, and a mortality rate characteristic of a long-lived strategy within tropical ecosystems. In addition, the same hydraulic parameters were used across all sites to maintain same representation of plant water transport (Xu et al., 2016). To represent local differences in physiological and structural parameters, five parameters, the density of the wood, the root-to-leaf area ratio, the maximum leaf area index, the mortality rate and the leaf area per mass, were tuned to match observational data. These variations enable the model to represent a range of plausible plant responses while preserving a consistent functional identity. By integrating these mechanistic representations, BiomeE captures key ecological processes such as carbon allocation, competition for resources, and physiological constraints under climate extremes. The use of a single PFT reduces model complexity while preserving critical ecological dynamics in tropical forests. However, it is acknowledged that incorporating multiple PFTs could provide a more nuanced representation of species diversity and competitive interactions.

2.2 Study Areas and Meteorological Data

To account for the variability of baseline climate conditions, three tropical forest sites spanning a precipitation gradient were selected. These sites have comprehensive datasets that describe the forest structure, long-term climate conditions, and ecosystem functional properties, as described below.

Barro Colorado Island (BCI) is a 1,560-hectare island located in Gatun Lake, Panama, covered by evergreen broadleaf tropical moist forest. The mean annual temperature is 26^{o}C, with a 4- to 5-month dry season (mid-December to April). Annual precipitation averages 2612 mm (Windsor, 1990), and relative humidity remains high (80–90%). The BCI climate dataset spans from 01 January 1972 to 31 December 2021 and combines long-term records of rainfall and temperature with additional meteorological variables (e.g., radiation, humidity) required to drive BiomeE. The PFT used in BiomeE at this site has a high

https://doi.org/10.5194/egusphere-2026-145
Preprint. Discussion started: 5 February 2026

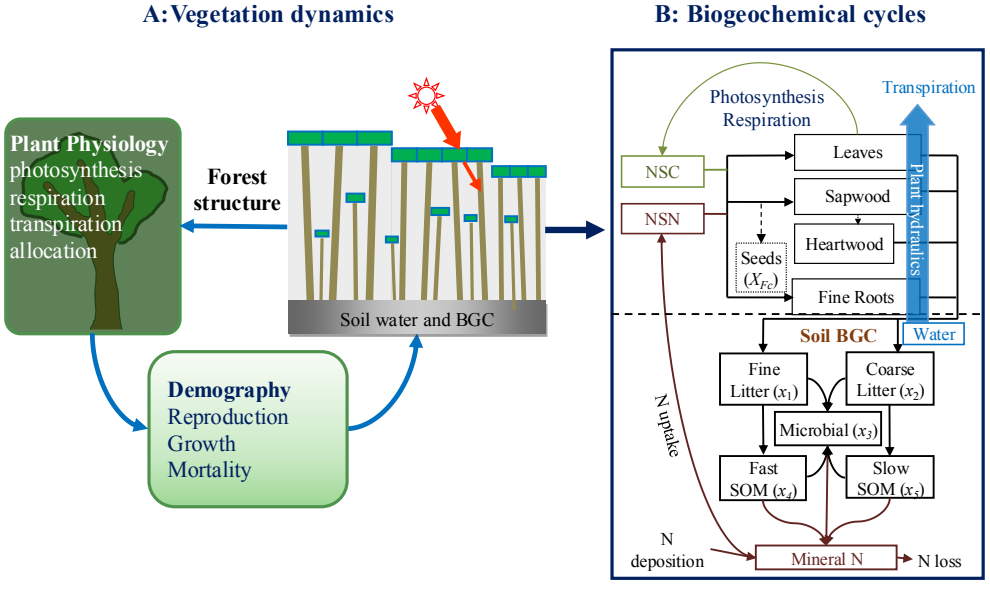

Figure 1. Schematic representation of BiomeE, illustrating the key vegetation, biogeochemical, and hydraulic processes simulated by the model. (A) Vegetation structure and dynamics, where plant cohorts compete for light, water, and nutrients, driving demographic processes such as growth, reproduction, and mortality. Tree canopies are arranged into vertical layers based on height and crown area, following the perfect plasticity approximation (PPA) framework. (B) Biogeochemical structure, depicting carbon, nitrogen, and water pools and their respective fluxes. Green arrows represent carbon fluxes, brown arrows indicate nitrogen fluxes, and blue arrows show water fluxes, including transpiration, soil water movement, and plant hydraulic processes.

wood density (436 kg/m^3), a root-to-leaf area ratio of 2.0, and a maximum LAI of 4.5, reflecting a resource-conservative strategy with enhanced drought tolerance. The low mortality rate (0.02 year^{-1}) and relatively high LMA (0.072) suggest a long-lived strategy with moderate growth rates.

The GuyaFlux (GYF) tower is located at the Paracou Field Station in French Guiana, within a 400-hectare area of tropical wet forest (Bonal et al., 2008). The mean annual temperature is 26^{o}C, and annual precipitation averages 3050 mm. A 3- to 4-month dry period (August to November) occurs annually, though humidity remains consistently high (80–90%). The GYF climate dataset spans from 01 January 1991 to 31 December 2020, providing meteorological records of temperature and precipitation. The PFT at this site has a wood density of 350 kg/m^3, a root-to-leaf area ratio of 1.2, and a maximum LAI of 3.5, representing a moderate balance between growth and survival strategies. The low mortality rate (0.0113 year^{-1}) and LMA of 0.072 support a long-lived, resource-efficient strategy with stable carbon allocation.

The Tapajos National Forest (TNF) is a protected evergreen forest in the Brazilian Amazon, characterized by a closed canopy with an average tree height of 40 meters (Rice et al., 2004). The mean annual temperature is 26^{o}C, with a 5-month dry season (mid-July to mid-December). Annual precipitation averages 1900 mm, and humidity remains high (80–90%) (Da Rocha

https://doi.org/10.5194/egusphere-2026-145
Preprint. Discussion started: 5 February 2026

et al., 2009). The TNF climate dataset spans from 01 January 1972 to 31 December 2021, providing meteorological records of temperature and precipitation. The PFT here has a lower wood density (300 kg/m^3), a root-to-leaf area ratio of 1.2, and a maximum LAI of 3.5, reflecting a more growth-oriented strategy compared to the other sites. The higher leaf nitrogen content (1.5E^{-3} kgN/m^2) supports greater photosynthetic capacity, while the low mortality rate (0.02 year^{-1}) ensures long-term persistence.

BiomeE was used to simulate annual Gross Primary Productivity (GPP) at each site (Supplementary Figure A1). The simulations were compared with available eddy covariance observations to assess whether the model reproduces basic productivity patterns under ambient conditions. While BiomeE captures site-specific differences in average GPP, it does not reproduce the full interannual variability observed at BCI, likely reflecting the absence of parameter calibration. This comparison therefore serves as a qualitative consistency check rather than a formal validation, since the study's goal is to examine the relative ecosystem responses to imposed climate stressors. Annual mean temperature and total precipitation were computed from the forcing data for each site and plotted as yearly time series (Supplementary Figure A2) to illustrate environmental differences relevant to forest functioning.

2.3 Simulated Climate Stressors

Following the collection of observational data from the tropical forest sites, several scenarios projecting climate extremes were applied to the data to inform the model's future predictions. These scenarios were designed to reflect plausible future climate conditions, based on observed patterns of drought and heatwave events in tropical regions and supported by projections from climate models and reports, such as the IPCC Sixth Assessment Report (Seneviratne et al., 2021). Similar patterns of increased drought frequency and intensity, as well as more frequent and severe heatwaves, have been documented in projections from CMIP6 models (Cook et al., 2020) and supported by studies highlighting the trend and spatial spread of climate extremes under warming scenarios (Adeyeri et al., 2022).

These projections consistently indicate that tropical regions will experience heightened climate extremes in the form of prolonged droughts and intense heatwaves as global temperatures rise. Specifically, drought conditions (changes in precipitation) and increased warming (changes in air temperature) were incorporated by modifying the respective datasets. This approach enables an assessment of how varying levels of climate extremes might impact tropical forest ecosystems over time, consistent with the types of changes projected under future climate scenarios.

To examine the influence of drought and warming extremes on ecosystem responses, modifications were applied to precipitation and temperature datasets at multiple temporal scales. Drought conditions were simulated by modeling the inter-arrival of dry spells as a Poisson process, and then increasing how long they last at the daily, seasonal, and interannual levels. Here, a dry spell refers to consecutive days (or years) with little rainfall, as discussed next. The durations of dry periods were systematically extended while maintaining the total number of dry and wet events. Rainfall was then reconstructed using characteristic dry-season patterns derived from observational data, allowing sub-daily and seasonal variability to be preserved. Warming scenarios were generated by applying a Fourier-based spectral transformation to the temperature time series, in which amplitudes were adjusted at selected frequencies to represent variability at daily (e.g., extreme heat events), annual (seasonal

https://doi.org/10.5194/egusphere-2026-145
Preprint. Discussion started: 5 February 2026

extremes), and multi-year (e.g., ENSO-scale) timescales. In addition to frequency-specific changes, the mean temperature was also modified to simulate uniform warming across the entire time series.

These perturbations enabled the creation of physically consistent climate forcing scenarios while retaining the other statistical properties of the original time series. Further methodological details are provided in the following subsections. Other meteorological variables, such as relative humidity and solar radiation, were kept constant to isolate the impacts of drought and warming, though it is acknowledged that changes in precipitation can influence light availability, relative humidity, and temperature. These modified datasets were used as model forcing for post-equilibrium simulations to assess long-term impacts on forest structure, carbon and water fluxes, and ecosystem resilience. An example of precipitation and temperature modifications used in the drought and warming scenarios is provided in Table C1.

2.3.1 Drought Scenarios

Three dry spell extension scenarios were developed to simulate potential future drought conditions at daily, seasonal, and yearly timescales. Each timescale was chosen to capture drought impacts operating over different durations and processes:

(i) *Daily Dry Spell Extension*: Short-term drought events were simulated by lengthening dry spells at the daily scale through geometric resampling of dry spell durations. This approach captures intermittent dry periods that can cause rapid plant water stress and hydraulic dysfunction.

(ii) *Seasonal Dry Spell Extension*: Large-scale droughts were modeled by increasing the duration of consecutive dry months based on monthly rainfall thresholds. This timescale represents prolonged dry periods that influence ecosystem water availability and phenology over seasonal cycles.

(iii) *Yearly Dry Spell Extension*: Longer-term drought variability, such as ENSO-driven dry years, was represented by extending dry years defined below a percentile rainfall threshold. Rainfall during added dry years was reconstructed to preserve seasonal and sub-seasonal variability by retaining each year's original monthly and daily fractions and applying an hourly template characteristic of dry years.

2.3.2 Air Temperature Scenarios

Four simplified warming scenarios were implemented to capture a range of potential thermal stresses under future climate change:

(i) *Daily Temperature Variability Increase* amplified high-frequency temperature variability by enhancing daily and hourly fluctuations, simulating short-term heat extremes that can affect plant physiological responses such as stomatal behavior or photosynthesis efficiency.

(ii) *Seasonal Temperature Amplification* increased temperature amplitude during the hottest season, representing seasonal-scale heat stress often linked to changes in phenology or evapotranspiration dynamics.

https://doi.org/10.5194/egusphere-2026-145
Preprint. Discussion started: 5 February 2026

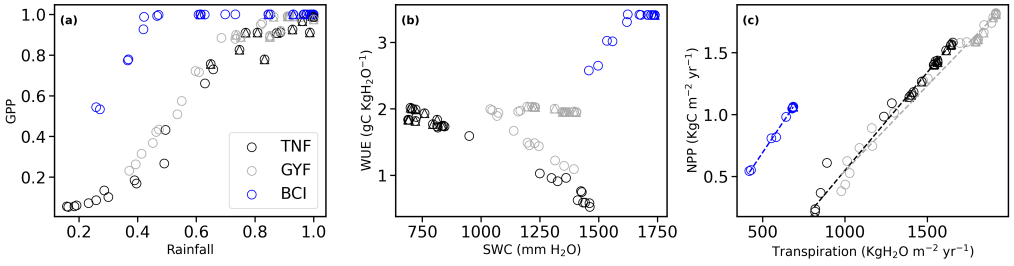

Figure 2. Impact of drought experiments on the three studied sites under current temperature conditions. Results are shown for Barro Colorado Island (BCI) in blue, Paracou (GYF) in gray, and Tapajos National Forest (TNF) in black. Daily extensions are shown in circles and yearly extensions are shown in triangles. Results are means across replicate simulations and over the perturbation window (30 years for BCI; 50 years for GYF and TNF) with error bars showing the standard error. (a) Average gross primary production (GPP; unitless, normalized by each site's current scenario) as a function of total rainfall (unitless, normalized by current scenario). (b) Average water use efficiency (WUE; gC kgH_2O^{-1}) as a function of average soil water content (SWC; mm H_2O). (c) Average net primary production (NPP; kgC m^{-2} yr^{-1}) as a function of average transpiration (kgH_2O m^{-2} yr^{-1}).

(iii) *Multi-year Temperature Oscillation Increase* enhanced low-frequency variability over multi-year timescales (3–7 years), capturing temperature oscillations analogous to ENSO-like patterns and their influence on long-term ecosystem functioning.

(iv) *Mean Temperature Offset Increase* introduced a uniform warming across the entire time series, representing long-term shifts in baseline climate.

While future warming means higher temperatures during both day and night, the variability scenarios (i–iii) were simply meant as controlled extensions of temperature variability to test how the ecosystem responds across timescales. Future work will look into adding an overall warming trend together with this extended variability. These scenarios allow the decoupled assessment of different warming frequencies and their potential ecological impacts in tropical forests. These scenarios allow assessment of drought impacts across temporal scales relevant to plant physiology, ecosystem dynamics, and climate variability.

Detailed methodology and algorithmic implementation for each scenario are provided in Supporting Information B and C. Illustrative examples of the precipitation modifications summarized in Table C1 are shown in Supplementary Figure C1, which demonstrates how daily, seasonal, and yearly dry-spell extensions alter rainfall distributions at BCI. Supplementary Figure C2 illustrates the warming scenarios summarized in Table C1, showing how amplifying different spectral components or applying a mean offset modifies temperature variability across daily, seasonal, and interannual timescales.

https://doi.org/10.5194/egusphere-2026-145
Preprint. Discussion started: 5 February 2026

3 Results

3.1 Drought impacts across sites and scenarios

In Figure 2, drought responses are plotted against multiple water-stress metrics (rainfall, soil water content, and transpiration) to distinguish changes in external water supply from shifts in internal hydraulic transport. Across all sites, GPP remained stable under relatively high precipitation and declined rapidly once rainfall fell below a site-specific threshold (Figure 2a). The location of this threshold differed markedly between BCI and the other two forests. At TNF and GYF, GPP began to decline when rainfall dropped to roughly 80% of ambient conditions. In contrast, BCI maintained high GPP until precipitation was reduced by nearly 60% (rainfall ≈ 0.4), indicating substantially greater drought tolerance.

Figure 2(b) shows that these GPP patterns correspond to distinct water-use strategies across sites. At BCI, average WUE was consistently higher than at GYF and TNF and remained stable until water supply became strongly limiting, reflecting tight stomatal regulation. In contrast, TNF exhibited increasing WUE as rainfall declined, GPP was maintained longer than transpiration, suggesting a more anisohydric strategy that keeps stomata open under increasing water stress. GYF showed a mixed response: WUE remained relatively flat under non–water-limited conditions (especially in the yearly drought scenarios, triangles), but under daily drought (circles) it followed the TNF-like pattern, with transpiration decreasing faster than GPP and thus rising WUE.

Transpiration–NPP relationships further illustrate these site differences (Figure 2c). BCI consistently maintained lower transpiration and lower NPP than the other sites and showed the steepest decline in NPP per unit decrease in transpiration (slope $= 0.00198$, $R^2 = 0.997$) , consistent with its decreasing WUE at low water supply. GYF and TNF showed shallower slopes (0.00138 and 0.00158, with $R^2 = 0.987$ and $R^2 = 0.982$, respectively), but the linear fit obscures a sharp downturn in TNF's results once transpiration drops below $\sim 1000\ \mathrm{kg, H_2O, m^{-2}, yr^{-1}}$. This nonlinear collapse is consistent with the abrupt decline in GPP at low rainfall in Figure 2(a), indicating near-shutdown of ecosystem carbon uptake.

3.2 Warming effects across sites and scenarios

Figure 3(a) shows that all sites experience an initial decline in GPP under warming, but the magnitude and threshold of decline differ across sites. GYF exhibits the earliest decline, with GPP dropping rapidly at approximately a 15% increase in temperature (about $4°C$), eventually reaching a 90% reduction from ambient conditions. At BCI, the corresponding decline begins near a 16–17% increase in temperature, and no ecosystem collapse is observed within the tested range. TNF maintains relatively higher GPP values over the same range and shows a nearly linear decline with increasing warming. These site differences are more apparent in Figure 3(b), where GYF shows an 80% reduction in GPP earlier than the other sites, while BCI remains near ambient for most of the warming range.

Figure 3(c) shows that TNF experiences a sharp decline in GPP near a fourfold increase in temperature range. In contrast, GYF undergoes a more gradual decline over the same range. BCI shows a threshold near a sixfold increase in temperature range, after which GPP decreases more rapidly. Figures 3(d)–(f) indicate that warming events applied at longer periods (multi-

https://doi.org/10.5194/egusphere-2026-145
Preprint. Discussion started: 5 February 2026

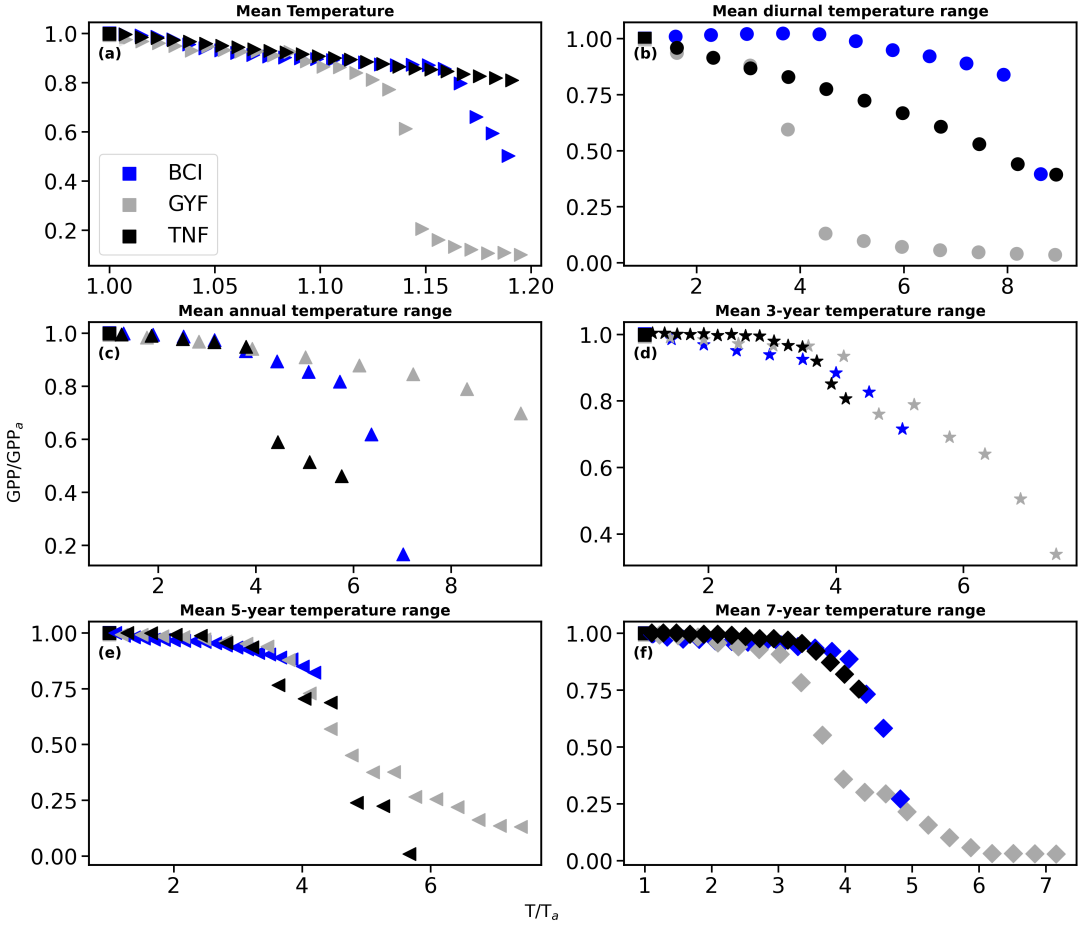

Figure 3. Impact of warming experiments on the three studied sites. Results are shown for BCI in blue, GYF in gray, and TNF in black. Squares denote the ambient case, the reference point at (1,1) in each panel. Each point is the yearly average over the perturbation window (30 years for BCI; 50 years for GYF and TNF) and normalized to that site's ambient case. Panels show normalized GPP as a function of (a) mean temperature (right triangle), (b) mean diurnal temperature range (circles), (c) mean annual temperature range (triangles), (d) mean 3-year temperature range (stars), (e) mean 5-year temperature range(left triangle), and (f) mean 7-year temperature range (diamonds).

https://doi.org/10.5194/egusphere-2026-145
Preprint. Discussion started: 5 February 2026

year) produce similar GPP decline rates across sites, with thresholds occurring near a fourfold increase in temperature range. An exception is GYF under the 7-year period (Figure 3(f)), where GPP declines earlier, around a 3.5-fold increase.

Figure 4 shows the effects of warming-event frequency on transpiration. At BCI (top panel), uniform hourly warming produces the largest reduction in transpiration. An increase in transpiration occurs at lower warming levels before a sharp decline. Daily warming (circles) results in a more gradual reduction in transpiration compared to longer-period warming events, which show an earlier decrease near a 110% increase in VPD relative to ambient. At GYF (middle panel), responses differ by timescale: seasonal warming (triangles) produces the slowest decline in transpiration, followed by the 3-year (stars), 5-year (left triangles), and 7-year (diamonds) warming periods. TNF (bottom panel) shows comparatively smaller differences across warming frequencies, with the uniform temperature increase (right triangles) maintaining higher transpiration over a broader range, consistent with Figure 3(a).

3.3 Cumulative effects of warming and drought

Figure 5 shows the effects of combined drought and warming events applied at the yearly timescale. In these simulations, warming was imposed at the 5-year period and drought at the yearly period (Sections 2.3.1 and 2.3.2). The left panels show that normalized GPP decreases more with increasing VPD with lower sensitivity to rainfall, except for TNF that shows the sharpest decline with rainfall. At GYF, the main decline occurs when maximum VPD exceeds about 1.6 of its ambient value, whereas rainfall alone produces weaker reductions. BCI shows smaller GPP reductions across the tested ranges.

The right panels of Figure 5 show the temporal evolution of GPP for three representative combinations of rainfall and VPD (indicated by the corresponding markers). At TNF, the two more extreme combinations lead to a rapid GPP decrease within one or two perturbation cycles, whereas the mildest case maintains GPP near ambient levels. At GYF, GPP decreases most strongly under the highest-VPD scenario, while the two milder cases remain close to ambient. At BCI, GPP remains relatively stable across all selected combinations.

Figure 6 shows the results for the combined drought and warming experiments at the daily timescale. Here, both warming and drought were imposed daily by increasing maximum daytime temperature and extending the number of dry days per year (Sections 2.3.2 and 2.3.1). The left panels show normalized GPP as a function of normalized VPD and rainfall. All three sites exhibit decreasing GPP with increasing VPD and decreasing rainfall, although BCI shows a slight increase under low-to-moderate VPD increases. At TNF, mean annual rainfall is substantially reduced relative to ambient, yet GPP remains above collapse thresholds except in the most extreme VPD–rainfall combination.

At GYF, normalized GPP decreases once VPD exceeds roughly 1.5 of current conditions, with rainfall deficits contributing additional reductions compared to the yearly-scale results. BCI shows modest GPP reductions, remaining within about 10% of ambient even under the highest VPD and lowest rainfall conditions. The right panels of Figure 6 present the cycle-averaged GPP time series for the selected combinations of VPD and rainfall. At TNF, only the most extreme stress combination shows a sustained decline in GPP, while the other two combinations produce reduced but stable productivity. At GYF, both the moderate and extreme VPD cases lead to lower GPP relative to ambient. At BCI, GPP remains close to ambient under mild increases in VPD and decreases modestly under stronger stress.

https://doi.org/10.5194/egusphere-2026-145
Preprint. Discussion started: 5 February 2026

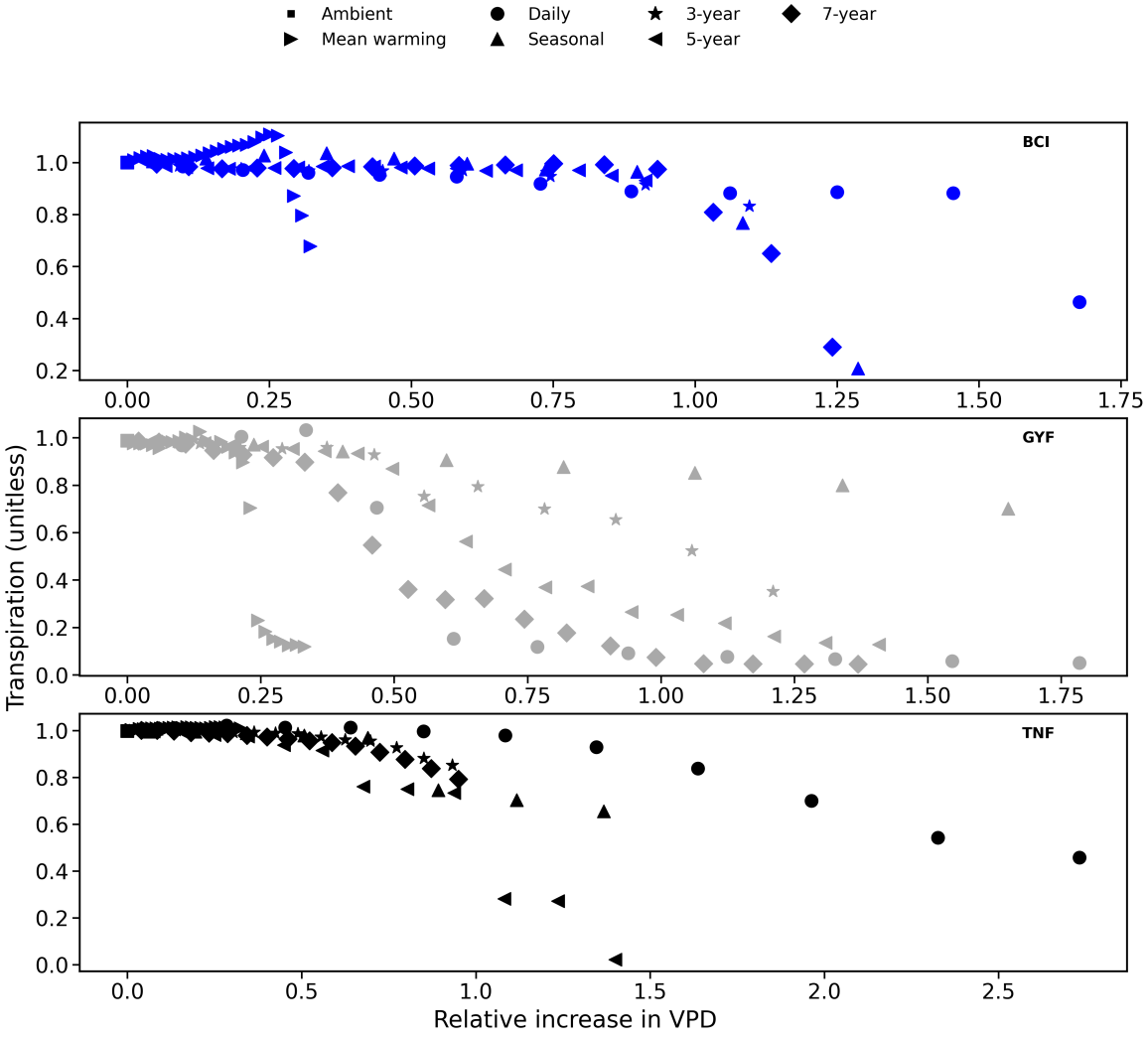

Figure 4. Yearly-averaged normalized transpiration, computed over the perturbation window (30 years for BCI; 50 years for GYF and TNF), as a function of relative increase of the maximum vapor pressure deficit to ambient conditions for the different warming scenarios at the three sites. Results are shown for BCI in blue in the top panel, GYF in gray in the middle panel, and TNF in black in the bottom panel. Squares denote the ambient case (the reference point at (1,1) in each panel), right triangles denote an increase in overall temperature (increase in the zeroth frequency in the Fourier domain), circles denote an increase in daily variability (1-day period), triangles denote an increase in seasonal variability (1-year period), stars denote an increase in yearly variability at the 3-year period, left triangles denote an increase in yearly variability at the 5-year period, and diamonds denote an increase in yearly variability at the 7-year period.

https://doi.org/10.5194/egusphere-2026-145
Preprint. Discussion started: 5 February 2026

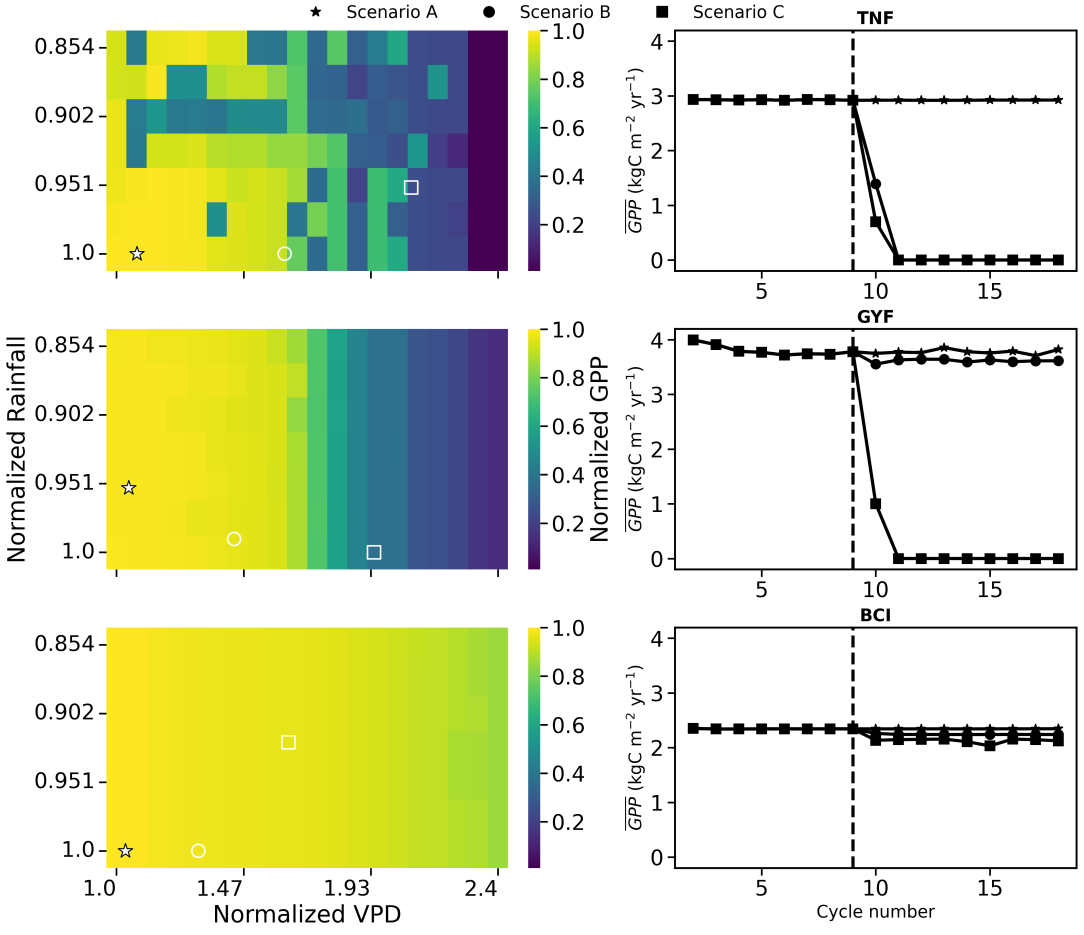

Figure 5. Results for the combined drought and warming (5-year period) experiments at the yearly scale. Left panels show the normalized gross primary production (GPP), averaged over the first perturbation cycle, as a function of normalized maximum vapor pressure deficit (VPD) and normalized rainfall, all relative to each site's current conditions. Symbols (star, circle, and square) mark the locations of three representative climate scenarios in VPD-rainfall space (A, B, and C). Right panels show the corresponding cycle-averaged GPP (kgC m^{-2} yr^{-1}) as a function of cycle number for the same three scenarios, using the same marker shapes as in the left panels to link forcing conditions to ecosystem responses. Results are averaged over the perturbation window (30 years for BCI; 50 years for GYF and TNF). The dashed vertical line marks the onset of the perturbation window separating the spin-up from the stressed period.

https://doi.org/10.5194/egusphere-2026-145
Preprint. Discussion started: 5 February 2026

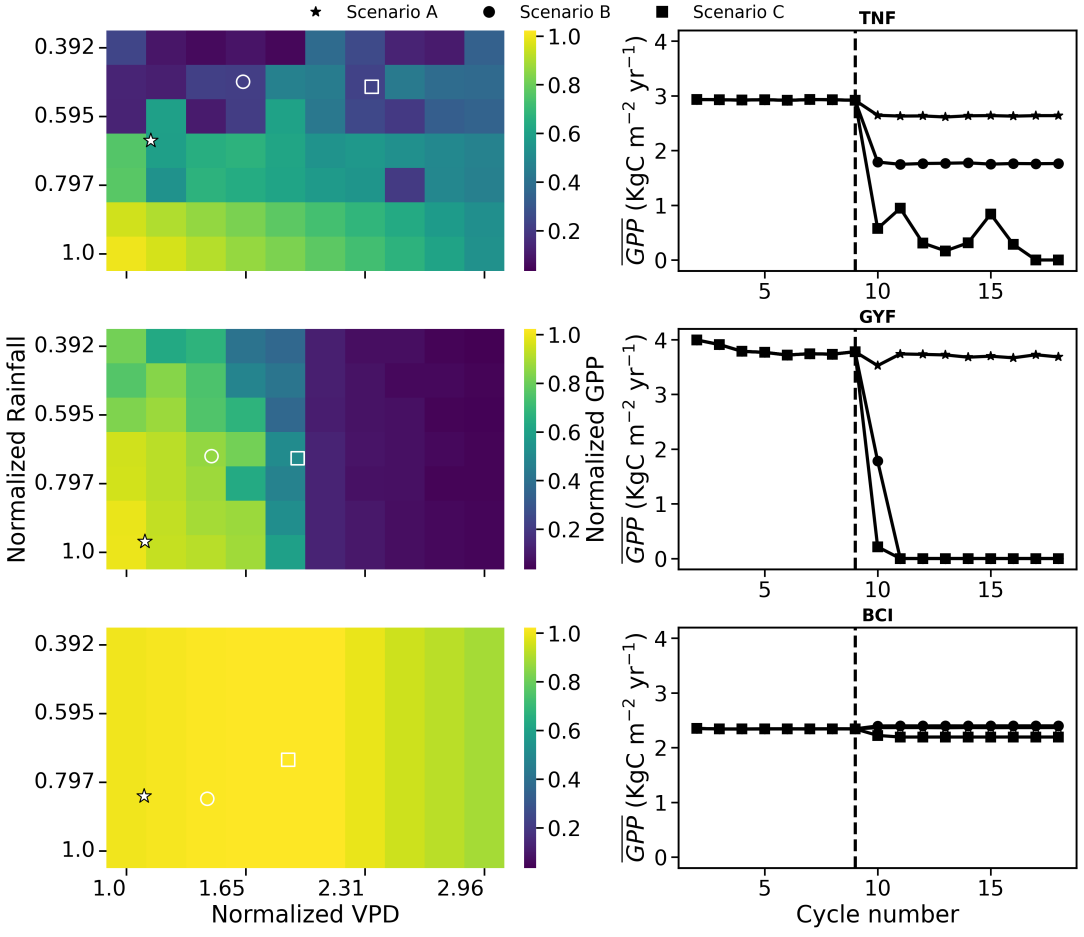

Figure 6. Results for the combined drought and warming experiments at the daily scale. Left panels show the normalized gross primary production (GPP), averaged over the first perturbation cycle, as a function of normalized maximum vapor pressure deficit (VPD) and normalized rainfall, all relative to each site's current conditions. Symbols (star, circle, and square) mark the locations of three representative climate scenarios in VPD-rainfall space (A, B, and C). Right panels show the corresponding cycle-averaged GPP (kgC m^{-2} yr^{-1}) as a function of cycle number for the same three scenarios, using the same marker shapes as in the left panels to link forcing conditions to ecosystem responses. Results are averaged over the perturbation window (30 years for BCI; 50 years for GYF and TNF). The dashed vertical line marks the onset of the perturbation window separating the spin-up from the stressed period.

https://doi.org/10.5194/egusphere-2026-145
Preprint. Discussion started: 5 February 2026

4 Discussion

4.1 Soil Moisture Limitation and Forest Stability

Tropical forests play a crucial role in the global carbon and water cycles, yet their response to climate extremes remains uncertain. This study evaluates how three contrasting tropical sites, Barro Colorado Island (BCI), Paracou (GYF), and Tapajos National Forest (TNF), respond to altered drought intensity, drought frequency, and warming, with the aim of identifying the mechanisms governing ecosystem stability.

BCI showed strong resilience, maintaining productivity even under a 50% year-round reduction in precipitation. This agrees with previous studies demonstrating that wet tropical forests can sustain GPP despite multi-year rainfall deficits (Nepstad et al., 2002; da Costa et al., 2010). TNF, with the driest baseline climate, exhibited larger GPP reductions under severe drought, consistent with the expectation that water-limited forests are more vulnerable (Longo et al., 2018). However, the scenarios explored here pushed all three sites further than past experiments, allowing threshold behavior to emerge in wetter forests such as GYF.

Across sites, drought impacts emerged only once rainfall fell below specific thresholds, confirming that cumulative water supply determines when ecosystems begin to decline. TNF and GYF showed similar relative sensitivities: GPP began declining when rainfall dropped by about 20% from ambient conditions. However, because GYF receives much higher baseline rainfall, this same fractional reduction corresponds to a substantially higher absolute rainfall level. Consequently, GYF's GPP begins collapsing at higher absolute rainfall than TNF, indicating that GYF requires more absolute water to sustain productivity. Yet despite this higher sensitivity, only TNF reached full ecosystem collapse under the strongest drought sequences, because its initial soil water reservoir is far smaller. GYF, even after losing 60% of its rainfall, still retains more water in absolute terms, allowing the ecosystem to persist. BCI remained the most drought-resilient overall.

These differences are linked to contrasting water-use strategies and hydraulic behavior. In the simulations, BCI exhibits tighter stomatal regulation and consistently higher WUE, reducing transpiration early and maintaining closer coupling between GPP and water loss. This prevents the rise in WUE that characterizes stress responses at the other two sites. In contrast, GYF and TNF allow transpiration to remain high as soils dry, causing WUE to increase because transpiration declines faster than GPP. This anisohydric tendency increases short-term carbon gain but elevates hydraulic risk once soil moisture falls below a critical threshold. TNF is especially vulnerable: when transpiration drops below roughly $\sim 1000\,\mathrm{kg, H_2O, m^{-2}, yr^{-1}}$, hydraulic conductance declines sharply, producing the nonlinear downturn observed in both GPP and NPP.

Overall, these patterns show that soil moisture limitation is the primary driver of ecosystem instability in BiomeE. Once the soil reservoir is depleted, recovery depends on the plant's hydraulic capacity and site-specific water-use strategy. The increasing frequency and intensity of droughts projected under future climate scenarios (Robbins et al., 2024) highlight the importance of mechanistic hydraulic models for predicting tropical forest vulnerability. In this context, the results here clarify that GYF is more sensitive in absolute terms, TNF is more collapse-prone due to lower baseline water supply, and BCI is the most resilient owing to conservative water use and high rainfall.

https://doi.org/10.5194/egusphere-2026-145
Preprint. Discussion started: 5 February 2026

4.2 Atmospheric Water Demand and the Role of Vapor Pressure Deficit

Warming primarily influenced ecosystem function through increases in vapor pressure deficit (VPD), which raised atmospheric water demand and reduced GPP across all sites (Lin et al., 2025). Because pressure and relative humidity were held constant, higher air temperature directly elevated VPD and intensified evaporative demand. Unlike drought, which limits water supply to the roots, warming acts on the demand side: leaves lose more water for the same soil moisture level, increasing xylem tension and reducing stomatal conductance (Grossiord et al., 2020). Although BiomeE does not include thermal acclimation or temperature-dependent adjustments of leaf traits, the simulations show that hydraulic stress and productivity losses can occur even when soil moisture remains high, purely because of excessive atmospheric demand (Bauman et al., 2022).

The ecosystem responses differed substantially across sites. GYF was the most warming-sensitive: GPP declined rapidly once temperatures rose beyond roughly $4°C$ above ambient, leading to ecosystem collapse. BCI maintained productivity over a larger warming range, with declines occurring only under stronger forcing. TNF showed the slowest decline and remained the most resilient of the three sites. These differences reflect how warming interacts with baseline climate. In wetter systems (BCI and GYF), the higher initial transpiration amplifies the VPD-driven water loss, causing earlier stomatal regulation and pronounced declines in GPP (Detto and Pacala, 2022). TNF, with lower baseline transpiration and atmospheric demand, exhibited a more gradual, nearly linear response to warming.

The timescale of warming also strongly shaped ecosystem behavior. Short daily warming events generated sharp but brief VPD pulses, allowing partial hydraulic and carbon recovery between successive hot–dry periods. This buffering prevented immediate collapse at both BCI and GYF and produced the slower decline in transpiration seen in the Results. Hourly warming, in contrast, induced the strongest reductions in transpiration and GPP. Because thermal stress was applied continuously, ecosystems had no recovery window, causing an initial increase in transpiration at low warming levels followed by a rapid, sustained decline as evaporative demand exceeded hydraulic supply (Bartlett et al., 2016).

At longer periods (seasonal to multi-year), warming persisted for months and produced similar thresholds across sites, aligning with the fourfold increase in temperature range identified in the Results. This reflects the cumulative nature of prolonged thermal stress: although the amplitude of warming is the same, longer forcing windows expose the plant to elevated VPD for extended periods, exhausting hydraulic margins (Allen et al., 2010). GYF showed an earlier decline under multi-year warming (particularly at the 7-year timescale), consistent with its sensitivity to sustained evaporative demand.

4.3 Compound Effects of Drought and Warming

When drought and warming occurred together, warming amplified drought impacts by increasing VPD and raising atmospheric water demand. This intensified hydraulic strain across all sites, but the magnitude and timing of the response depended strongly on baseline hydroclimate and, critically, on the persistence of the combined stress.

The compound experiments showed that yearly-scale warm–dry conditions produced the most severe outcomes. Under these sustained events, GPP declined monotonically at all sites, with TNF undergoing rapid collapse once rainfall and VPD crossed their respective thresholds. Because warming and drought co-occurred for long periods, hydraulic stress accumulated

https://doi.org/10.5194/egusphere-2026-145
Preprint. Discussion started: 5 February 2026

and exceeded each ecosystem's capacity to maintain transpiration and carbon uptake. Notably, in the yearly compound case, ecosystem response was dominated by VPD, with rainfall playing only a secondary role in determining GPP declines.

In contrast, daily-scale compound events produced markedly different behavior. Although these scenarios generated lower mean annual rainfall and higher mean VPD, the short duration of each hot–dry pulse allowed partial recovery between events. As a result, TNF maintained productivity across most combinations and collapsed only in the most extreme case. This reversal relative to the yearly experiments highlights that stress duration, rather than intensity alone, governs ecosystem failure.

BCI remained the most resilient site under both timescales, with only modest GPP reductions and little sensitivity to rainfall deficits even at high VPD. Its slight increase in GPP under mild daily-scale VPD increases is consistent with improved water-use efficiency under moderate stress. GYF fell between BCI and TNF in overall sensitivity but displayed similar timescale-dependent behavior: strong declines under sustained yearly stress and more moderate responses under daily fluctuations.

Together, these results show that compound heat–drought impacts cannot be inferred from drought or warming in isolation. Instead, ecosystem stability depends on the interaction between soil moisture supply, atmospheric water demand, and the temporal structure of the forcing. Forests are more likely to collapse when warm–dry conditions persist continuously, whereas intermittent extremes allow hydraulic and carbon recovery that can delay or prevent failure.

4.4 Model Limitations and Future Directions

While these experiments provide mechanistic insight into how stress persistence and compound drought–warming interactions shape tropical forest stability, several limitations of the modeling framework should be noted. First, the BiomeE model assumes fixed carbon allocation parameters and does not capture adaptive shifts in allocation (e.g., changes in root-to-shoot ratio). Second, the model does not account for physiological acclimation to repeated or sustained stress, such as adjustments in photosynthetic capacity or hydraulic traits, which is a typical behavior for plant survival (Nakad et al., 2023). Third, the study holds relative humidity constant, neglecting potential co-variations among temperature, humidity, and radiation that could alter VPD and the surface energy balance under warming. Fourth, the simulations omit radiative effects from canopy loss, where reductions in LAI could increase soil evaporation and local heating, amplifying water loss during drought. Finally, no drainage or lateral water redistribution was included, which may influence soil moisture persistence after rainfall events. These simplifications limit the realism of the absolute magnitudes of the responses, although the relative patterns across sites and timescales are expected to remain robust.

BiomeE explicitly resolves size structure, canopy layering, and demographic processes, but in this study the analysis was restricted to ecosystem fluxes (GPP, NPP, transpiration), which are used as leading indicators of instability. Detailed examination of changes in biomass, stand structure, and mortality patterns under repeated extremes is beyond the scope of this work and is left for future studies. Resilience is interpreted here in terms of the persistence or collapse of carbon fluxes under sustained forcing regimes, rather than through formal metrics of recovery time or hysteresis following discrete shocks. In addition, although the model includes an explicit plant hydraulic scheme, xylem water potentials and loss of conductivity were not analyzed directly, and changes in transpiration and water-use efficiency were instead used as proxies for increasing hydraulic stress. Together, these choices define the scope of inference and highlight model components that warrant more detailed analysis.

https://doi.org/10.5194/egusphere-2026-145
Preprint. Discussion started: 5 February 2026

Future work should therefore aim to disentangle the relative roles of atmospheric demand and soil water supply in driving hydraulic failure. Determining whether mortality arises primarily from high VPD or from water depletion would improve predictions of forest vulnerability, particularly under future climates where both stressors intensify. The potential compensating effects of light availability under drought also warrant examination, since reduced cloud cover could enhance photosynthetic radiation but at the cost of greater evaporative demand. Incorporating such interactions, together with acclimation processes and dynamic carbon allocation, will help refine model thresholds separating recovery from collapse. Beyond climatic stressors, shifts in disturbance regimes such as storms and fires, as well as deforestation, logging, and other types of land-use and land-cover change, should also be considered to broaden the relevance of these simulations and strengthen predictions of tropical forest feedbacks to the global carbon–climate system. Overall, the present analysis provides a foundation for future work on species diversity, competition dynamics, and adaptive strategies, and underscores the critical role of mechanistic vegetation modeling as an essential tool for exploring and predicting ecosystem responses to climate extremes.

5 Conclusions

This study used the vegetation demography model BiomeE to examine how three tropical forest sites (BCI, GYF, and TNF) respond to changes in water supply (rainfall) and atmospheric water demand (VPD), imposed independently and in combination across multiple time scales. Across sites, productivity losses emerged only after rainfall dropped below site-specific thresholds, highlighting that cumulative water supply governs the onset of ecosystem decline. Differences in baseline hydroclimate and soil water storage produced contrasting vulnerabilities: TNF was the most collapse-prone under sustained drought due to limited initial water reserves, whereas BCI was consistently the most resilient, and GYF showed higher sensitivity in absolute rainfall terms but remained buffered by higher baseline precipitation.

Warming acted primarily through increased VPD, reducing GPP even when soil moisture remained relatively high, and the magnitude of the response depended strongly on baseline transpiration and on the persistence of the thermal forcing. Compound warming-drought experiments further demonstrated that ecosystem failure is controlled not only by stress intensity but also by stress duration: sustained yearly-scale warm and dry conditions produced the strongest declines, while intermittent daily-scale extremes allowed partial recovery and delayed collapse. Together, these results emphasize that tropical forest stability under climate extremes depends on the interaction between soil moisture supply, atmospheric demand, and the temporal structure of forcing, motivating the use of mechanistic demographic-hydraulic models to explore thresholds and site-dependent vulnerability under future climates.

Code and data availability. The model code and scripts used in this study are available at: https://doi.org/10.5281/zenodo.17625235

https://doi.org/10.5194/egusphere-2026-145
Preprint. Discussion started: 5 February 2026

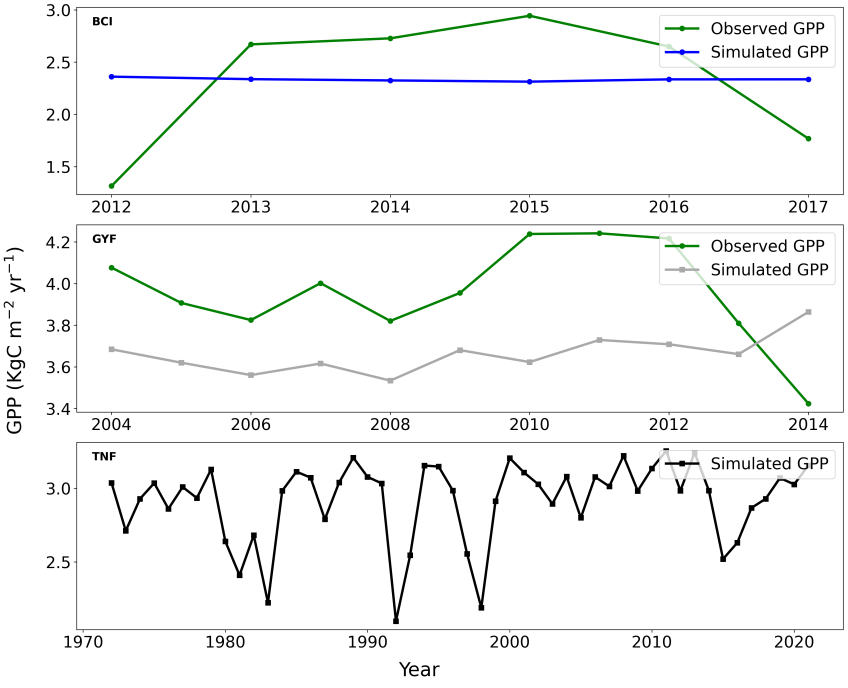

Figure A1. Annual Gross Primary Productivity (GPP) at the three tropical forest sites. Observed eddy covariance GPP is shown in green, while simulated GPP is shown for (a) BCI in blue, (b) GYF in grey, and (c) TNF in black.

Appendix A: Site-Level Observations of GPP and Climate Variables

Figure A1 presents the annual Gross Primary Productivity (GPP) at the Paracou Field Station in French Guiana (GYF) and Barro Colorado Island (BCI), based on both observed eddy covariance data (Bonal et al., 2008; Condit et al., 2019) and BiomeE simulations. The comparison illustrates that the model captures interannual variability and overall productivity trends reasonably well, particularly at the BCI site. For the Tapajos National Forest (TNF), only simulated GPP is shown due to the lack of available observational data. However, when compared with previously published values (Longo et al., 2018), the simulated average annual GPP is consistent with reported observations (see Figure S2 in the referenced study). It is important to note that the goal of this study is not to achieve accurate GPP predictions with BiomeE, but rather to explore the model's ability to simulate the impacts of drought and warming on tropical forests. Achieving high predictive accuracy would require a data assimilation approach, where observational data are used to constrain key model parameters, such as the maximum carboxylation rate (V_{cmax}). This parameter calibration lies beyond the scope of the present work.

Figure A2 illustrates the annual variations in mean temperature and total precipitation across the three sites: GYF (Paracou Field Station), BCI (Barro Colorado Island), and TNF (Tapajos National Forest). The Tapajos site consistently receives the lowest total rainfall under ambient conditions, making it particularly susceptible to drought stress, as discussed in the main text. In contrast, GYF experiences relatively lower mean temperatures, which likely correspond to lower vapor pressure deficits

https://doi.org/10.5194/egusphere-2026-145
Preprint. Discussion started: 5 February 2026

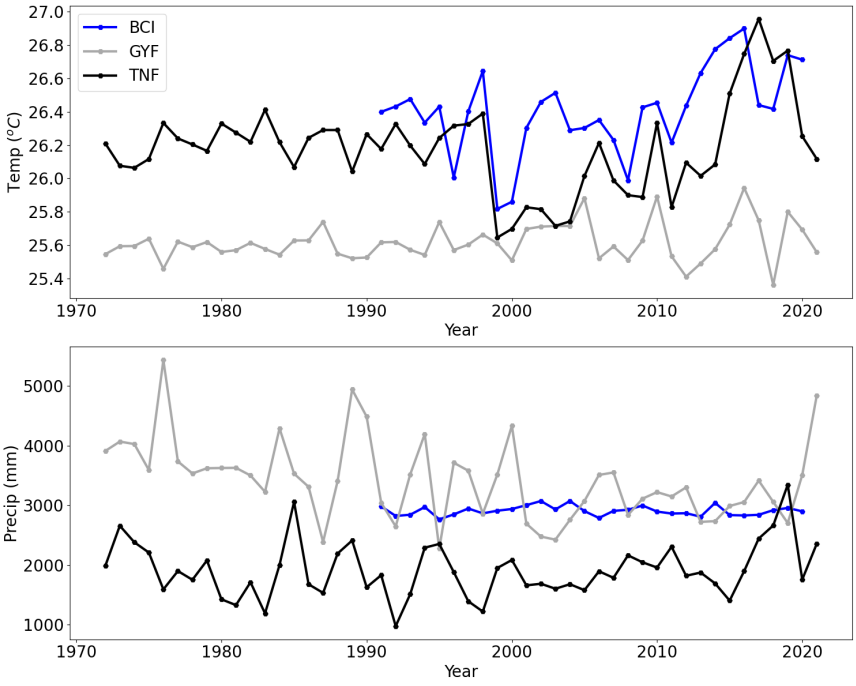

Figure A2. Annual mean temperature (top) and total precipitation (bottom) at the three tropical forest sites: BCI (blue), GYF (grey), and TNF (black).

(VPD), contributing to its heightened sensitivity to warming scenarios. These differences in climatic drivers are essential for interpreting site-level forest dynamics and simulation outcomes. The figure highlights how distinct baseline climate regimes shape the forest's vulnerability to environmental perturbations, reinforcing site-specific discussions presented earlier in the main text.

Appendix B: Detailed methodology of dry spell extension scenarios

The daily dry spell extension approach involved extending dry periods at the daily scale by resampling dry spell durations using a geometric distribution. First, daily total rainfall was calculated for each day of the year, and days with rainfall less than 1% of the mean daily rainfall were classified as dry. Consecutive dry days were grouped together to identify individual dry spells, and their lengths were recorded. For each dry spell, a new length was randomly sampled from a geometric distribution with a probability parameter inversely proportional to the product of the original dry spell length and a frequency scaling factor (for example, 2). This procedure effectively elongates dry spells by randomly increasing their duration while maintaining natural variability. The resampled dry spell lengths were then sequentially applied to reconstruct a modified dry/wet daily sequence, ensuring that no dry spells overlapped or exceeded the available data range. To reflect these changes in rainfall, all rainfall amounts on days classified as dry in the extended sequence were set to zero, while the original hourly rainfall distributions

https://doi.org/10.5194/egusphere-2026-145
Preprint. Discussion started: 5 February 2026

were preserved on wet days. In practice, this modification was imposed in years separated by a fixed recurrence interval controlled by the intensity parameter, and totals were not rescaled (i.e. the annual precipitation was affected by the increase in dry days). This method simulates short-term drought intensification by lengthening dry periods at a fine temporal resolution, which is critical for capturing rapid fluctuations that impact plant water stress and short-term hydrological dynamics.

At the seasonal scale, the methodology aimed to model prolonged drought events that influence seasonal water availability. Total monthly rainfall was computed for each month and year, and months with rainfall below 25% of the average monthly rainfall were flagged as dry. This threshold was selected because, on average, approximately one quarter of the months in the study period are characterized by notably low rainfall, effectively representing the seasonal minimum in precipitation. This fixed threshold was chosen as a site-specific indicator of very low monthly rainfall and does not imply that approximately one quarter of the months are flagged. By identifying months classified as dry under this threshold, the method realistically captures the typical timing and severity of seasonal drought conditions. Consecutive dry months were then grouped to define dry spell sequences and their lengths. These sequences were extended by multiplying the original spell lengths by a frequency scaling factor (e.g., 1.5), producing a modified dry/wet classification across the time series. For months that were originally wet but reclassified as dry, rainfall was reallocated daily fractions from that month's original series and an hourly template derived from original dry months. This redistribution preserved the within-month rainfall structure while simulating the impact of prolonged seasonal dryness. By extending dry spells at the seasonal timescale, this approach captures larger-scale droughts that can influence ecosystem processes such as phenology, soil moisture dynamics, and vegetation stress.

For the yearly dry spell extension, the focus was on capturing multi-year drought variability, such as that associated with El Nino Southern Oscillation (ENSO) events. Annual total rainfall was calculated for each year, and years with rainfall below the 20th percentile were identified as dry years. This threshold was selected to identify the most anomalously dry years while ensuring sufficient representation for statistical resampling. Consecutive dry years were grouped to determine dry spell lengths at the annual scale. These lengths were then resampled using a geometric distribution, where the probability parameter was inversely related to the product of the original dry spell length and a frequency factor. This resampling generated longer dry year sequences that mimic extended drought periods. The reconstructed yearly dry/wet sequence was then applied accordingly. For years that were added as dry in the modified sequence but were originally wet, rainfall was resynthesized to preserve seasonal and sub-seasonal variability by retaining each year's original monthly and daily fractions and applying an hourly template characteristic of dry years. An intensity scaling factor was also applied to simulate changes in drought severity. This yearly scale approach effectively captures prolonged drought events driven by large-scale climate variability, which are critical for understanding ecosystem resilience and long-term water resource dynamics.

The experiments spanned three timescales: daily, seasonal, and yearly. For each timescale, the duration of dry-period was extended as described above. Because the new dry-down lengths are random, the number of dry days per year (daily case) and the number of dry years (yearly case) varies even for the same factor. To account for this variability, 20 replicate simulations were run at each imposed dry-down intensity. Results were averaged across the 20 replicates and over the first atmospheric cycle after drought onset. Specifically, for GYF and TNF (50-year forcing files), simulations span 900 years and the reported averages are for years 450–500; for BCI (30-year forcing file), simulations span 540 years and the reported averages are for

https://doi.org/10.5194/egusphere-2026-145
Preprint. Discussion started: 5 February 2026

years 270–300. At the seasonal scale, the dry season could not be extended beyond six months, and under that extension the impact on annual rainfall was minimal. When annual rainfall was reduced, the results were consistent with the daily and yearly cases; therefore, seasonal results are omitted from the main figures. In cases where extreme drought (20–30% of current value) caused both annual transpiration and GPP to drop to zero, WUE was set to zero for averaging consistency.

Appendix C: Detailed methodology of warming scenarios

To generate the warming scenarios, a spectral modification approach was employed using the Fast Fourier Transform (FFT) to decompose the temperature time series into frequency components. This approach enables the isolation and amplification of variability at different timescales (e.g., daily, seasonal, multi-year), thereby allowing precise control over the type of thermal stress applied. After modification, the signal was reconstructed by applying the inverse Fourier transform to return to the time domain. All scenarios were applied to the same baseline hourly temperature dataset to ensure comparability across experiments.

For the Daily Temperature Variability Increase, high-frequency components of the temperature signal were targeted to simulate short-term heat extremes. The Fourier transform was applied to the original time series, and spectral energy corresponding to daily frequency (1 cycle per day) was selectively amplified by a fixed scaling factor. This enhanced short-term variability without altering lower-frequency trends or the overall mean. The Seasonal Temperature Amplification scenario focused on modifying temperature variability at the annual frequency to simulate enhanced warming during the hottest part of the year. This was achieved by amplifying the amplitude of the frequency component corresponding to one cycle per year in the Fourier domain. This adjustment increased the seasonal amplitude of the temperature signal, i.e., making hot seasons hotter, while preserving the timing and structure of the seasonal cycle. The Multi-year Temperature Oscillation Increase scenario enhanced interannual variability by increasing the spectral amplitude of low-frequency bands corresponding to 3, 5, and 7 year periods. These frequencies are characteristic of large-scale climate oscillations such as the El Nino–Southern Oscillation (ENSO), which influence regional climate regimes. After identifying the relevant spectral bins in the Fourier domain, their magnitudes were increased by a fixed factor to simulate stronger oscillatory behavior.

The Mean Temperature Offset Increase was implemented by modifying the zero-frequency (DC) component of the temperature spectrum, which represents the long-term average temperature. By increasing the amplitude of this component, a uniform temperature offset was applied across the entire time series, raising all hourly temperatures by a constant value. This scenario represents baseline warming driven by climate change and serves as a reference condition for assessing the additive or interactive effects of variability-based scenarios. Because only the mean was altered, short and long term variability remained unchanged, isolating the effects of elevated baseline temperature on ecosystem functioning. This frequency-domain approach allowed warming scenarios to be constructed in a modular and physically interpretable manner, with each modification targeting a specific ecological timescale. The resulting temperature time series preserves the overall temporal structure of the original climate data while simulating distinct warming regimes relevant to plant physiological thresholds, ecosystem phenology, and long-term climate responses.

https://doi.org/10.5194/egusphere-2026-145
Preprint. Discussion started: 5 February 2026

Simulations were run for the full forcing period (30 years for BCI; 50 years for GYF and TNF), and ecosystem outputs were averaged over the perturbation window following the initial equilibrium cycle. Warming was applied by widening the high–low while fixing the maximum above ambient at +20°C (the same constraint was used for all timescales). For analysis, the results were plotted against normalized temperature metrics: the mean temperature for the uniform offset scenario and the mean temperature range for the variability scenarios (daily, seasonal, and multi-year). For multi-year cases (3, 5, and 7 years), the temperature range was computed as the difference between the maximum and minimum temperature within each period and then averaged across the simulation window. All quantities were normalized by each site's ambient simulation for cross-site comparability. Examples of the modified time series for the uniform offset, daily, seasonal, and 3-year cases are shown in Supplementary Figure C2 (BCI).

Table C1. A sample of precipitation and temperature modifications applied in the drought and warming scenarios for BCI. Drought scenarios correspond to Figure C1, and warming scenarios correspond to Figure C2.

Scenario	Modification Applied	Factor
Drought Scenarios		
Daily Dry Spell Extension	Extend daily dry spells via geometric resampling	3
Seasonal Dry Spell Extension	Lengthen dry months by scaling consecutive dry months	2
Yearly Dry Spell Extension	Extend dry years (below 20th percentile) by geometric resampling	2
Warming Scenarios		
Daily Temperature Variability Increase	Amplify daily temperature variability (24-hour period in the Fourier domain)	3
Seasonal Temperature Amplification	Amplify annual temperature variability (365-day period in the Fourier domain)	10
Multi-year Temperature Oscillation Increase	Amplify multi-year temperature oscillations (example 3-year period in the Fourier domain)	100
Mean Temperature Offset Increase	Apply uniform warming via zero-frequency offset (Fourier domain)	+ 2^{o}C

https://doi.org/10.5194/egusphere-2026-145
Preprint. Discussion started: 5 February 2026

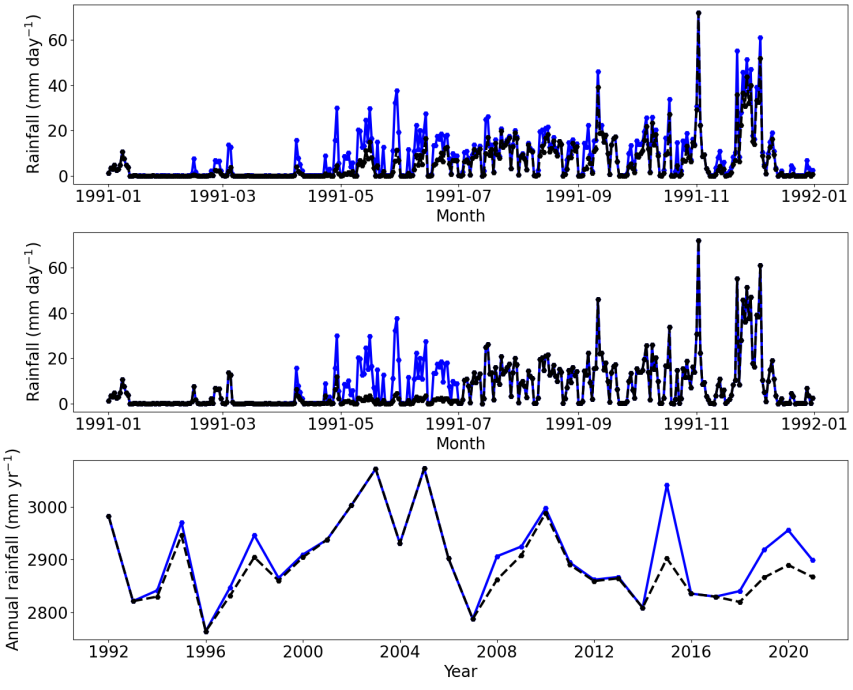

Figure C1. Drought scenarios for BCI as described in Table C1. Top panel shows the daily rainfall for the first year under ambient conditions (blue) and the Daily Dry Spell Extension (black dashed). Middle panel shows the daily rainfall for the first year under ambient conditions (blue) and the Seasonal Dry Spell Extension (black dashed). Bottom panel shows the annual rainfall totals under ambient conditions (blue) and the Yearly Dry Spell Extension (black dashed).

Author contributions. Conceptualization: MN, MM, MD, BIC, ZLY, PG, and EW. Data curation: MD, ML, GD, JL and EW. Formal analysis: MN, MD, and BIC. Funding acquisition: BIC, PG, and EW. Investigation: MN, MM, JK and TQ. Methodology: MN, MM, JK, and MD. Supervision: MN, BIC, PG, and EW. Validation and visualization: MN, MD, BIC, ML, GD, XX, JL, and EW. Writing (original draft preparation): MN and MM. Writing (review and editing): all authors.

Competing interests. The authors declare that they have no conflict of interest.

Acknowledgements. This work was supported by the NASA Modeling, Analysis, and Prediction (MAP) Program (Grant No. 80NSSC21K1496). MN acknowledges the startup support from the Lebanese-American University. An AI-based language tool (ChatGPT by OpenAI) was used solely to improve the readability and clarity of the manuscript.

https://doi.org/10.5194/egusphere-2026-145
Preprint. Discussion started: 5 February 2026

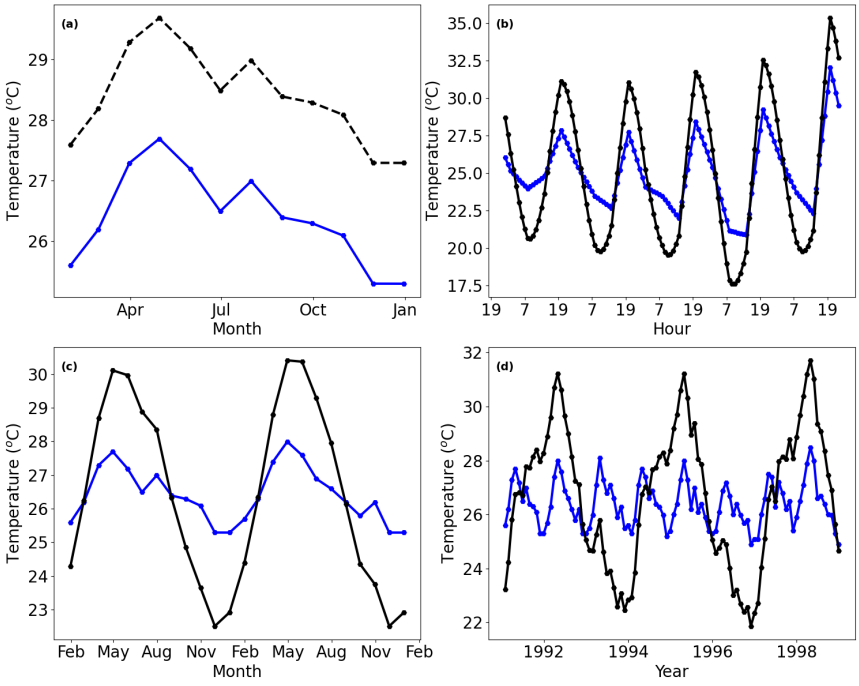

Figure C2. Warming scenarios for BCI as described in Table C1. (*a*) Monthly mean temperature for the first year under ambient conditions (blue) and Mean Temperature Offset Increase scenario (black dashed). (*b*) Diurnal temperature variations for ambient (blue) and Daily Temperature Variability Increase scenario (black dashed). (*c*) Monthly means for the first two years under ambient (blue) and Seasonal Temperature Amplification scenario (black dashed). (*d*) Monthly means for the first 8 years under ambient (blue) and Multi-year Temperature Oscillation Increase scenario (3 years in this case, black dashed).

References

Adeyeri, O. E., Zhou, W., Wang, X., Zhang, R., Laux, P., Ishola, K. A., and Usman, M.: The trend and spatial spread of multisectoral climate extremes in CMIP6 models, Scientific reports, 12, 21 000, 2022.

Allen, C. D., Macalady, A. K., Chenchouni, H., Bachelet, D., McDowell, N., Vennetier, M., Kitzberger, T., Rigling, A., Breshears, D. D., Hogg, E. T., et al.: A global overview of drought and heat-induced tree mortality reveals emerging climate change risks for forests, Forest ecology and management, 259, 660–684, 2010.

Bartlett, M. K., Klein, T., Jansen, S., Choat, B., and Sack, L.: The correlations and sequence of plant stomatal, hydraulic, and wilting responses to drought, Proceedings of the National Academy of Sciences, 113, 13 098–13 103, 2016.

Bauman, D., Fortunel, C., Delhaye, G., Malhi, Y., Cernusak, L. A., Bentley, L. P., Rifai, S. W., Aguirre-Gutiérrez, J., Menor, I. O., Phillips, O. L., et al.: Tropical tree mortality has increased with rising atmospheric water stress, Nature, 608, 528–533, 2022.

Bonal, D., Bosc, A., Ponton, S., GORET, J.-Y., Burban, B., Gross, P., BONNEFOND, J.-M., Elbers, J., Longdoz, B., Epron, D., et al.: Impact of severe dry season on net ecosystem exchange in the Neotropical rainforest of French Guiana, Global Change Biology, 14, 1917–1933, 2008.

https://doi.org/10.5194/egusphere-2026-145
Preprint. Discussion started: 5 February 2026

Bonan, G. B.: Forests and climate change: forcings, feedbacks, and the climate benefits of forests, science, 320, 1444–1449, 2008.

Bottino, M. J., Nobre, P., Giarolla, E., da Silva Junior, M. B., Capistrano, V. B., Malagutti, M., Tamaoki, J. N., de Oliveira, B. F. A., and Nobre, C. A.: Amazon savannization and climate change are projected to increase dry season length and temperature extremes over Brazil, Scientific Reports, 14, 5131, 2024.

Brienen, R. J., Phillips, O. L., Feldpausch, T. R., Gloor, E., Baker, T. R., Lloyd, J., Lopez-Gonzalez, G., Monteagudo-Mendoza, A., Malhi, Y., Lewis, S. L., et al.: Long-term decline of the Amazon carbon sink, Nature, 519, 344–348, 2015.

Ciais, P., Sabine, C., Bala, G., Bopp, L., Brovkin, V., House, J. I., et al.: Carbon and other biogeochemical cycles, in: Climate Change 2013: The Physical Science Basis. Contribution of Working Group I to the Fifth Assessment Report of the Intergovernmental Panel on Climate Change Change, pp. 465–570, Cambridge University Press, 2014.

Condit, R., Pérez, R., Aguilar, S., Lao, S., Foster, R., and Hubbell, S.: Complete data from the Barro Colorado 50-ha plot: 423617 trees, 35 years, (No Title), 2019.

Cook, B. I., Mankin, J. S., Marvel, K., Williams, A. P., Smerdon, J. E., and Anchukaitis, K. J.: Twenty-first century drought projections in the CMIP6 forcing scenarios, Earth's Future, 8, e2019EF001 461, 2020.

da Costa, A. C. L., Galbraith, D., Almeida, S., Portela, B. T. T., da Costa, M., de Athaydes Silva Junior, J., Braga, A. P., de Gonçalves, P. H., de Oliveira, A. A., Fisher, R., et al.: Effect of 7 yr of experimental drought on vegetation dynamics and biomass storage of an eastern Amazonian rainforest, New Phytologist, 187, 579–591, 2010.

Da Rocha, H. R., Manzi, A. O., Cabral, O. M., Miller, S. D., Goulden, M. L., Saleska, S. R., R.-Coupe, N., Wofsy, S. C., Borma, L. S., Artaxo, P., et al.: Patterns of water and heat flux across a biome gradient from tropical forest to savanna in Brazil, Journal of Geophysical Research: Biogeosciences, 114, 2009.

Detto, M. and Pacala, S. W.: Plant hydraulics, stomatal control, and the response of a tropical forest to water stress over multiple temporal scales, Global Change Biology, 28, 4359–4376, 2022.

Dybzinski, R., Farrior, C., Wolf, A., Reich, P. B., and Pacala, S. W.: Evolutionarily Stable Strategy Carbon Allocation to Foliage, Wood, and Fine Roots in Trees Competing for Light and Nitrogen: An Analytically Tractable, Individual-Based Model and Quantitative Comparisons to Data, The American Naturalist, 177, 153–166, https://doi.org/10.1086/657992, pMID: 21460552, 2011.

Farrior, C. E., Dybzinski, R., Levin, S. A., and Pacala, S. W.: Competition for Water and Light in Closed-Canopy Forests: A Tractable Model of Carbon Allocation with Implications for Carbon Sinks., The American Naturalist, 181, 314–330, https://doi.org/10.1086/669153, pMID: 23448882, 2013.

Feng, X., Uriarte, M., González, G., Reed, S., Thompson, J., Zimmerman, J. K., and Murphy, L.: Improving predictions of tropical forest response to climate change through integration of field studies and ecosystem modeling, Global change biology, 24, e213–e232, 2018.

Fisher, R. A., Koven, C. D., Anderegg, W. R., Christoffersen, B. O., Dietze, M. C., Farrior, C. E., Holm, J. A., Hurtt, G. C., Knox, R. G., Lawrence, P. J., et al.: Vegetation demographics in Earth System Models: A review of progress and priorities, Global change biology, 24, 35–54, 2018.

Flach, M., Brenning, A., Gans, F., Reichstein, M., Sippel, S., and Mahecha, M. D.: Vegetation modulates the impact of climate extremes on gross primary production, Biogeosciences, 18, 39–53, https://doi.org/10.5194/bg-18-39-2021, 2021.

Flack-Prain, S., Meir, P., Malhi, Y., Smallman, T. L., and Williams, M.: The importance of physiological, structural and trait responses to drought stress in driving spatial and temporal variation in GPP across Amazon forests, Biogeosciences, 16, 4463–4484, 2019.

Grossiord, C., Buckley, T. N., Cernusak, L. A., Novick, K. A., Poulter, B., Siegwolf, R. T., Sperry, J. S., and McDowell, N. G.: Plant responses to rising vapor pressure deficit, New phytologist, 226, 1550–1566, 2020.

https://doi.org/10.5194/egusphere-2026-145
Preprint. Discussion started: 5 February 2026

Hilker, T., Lyapustin, A. I., Tucker, C. J., Hall, F. G., Myneni, R. B., Wang, Y., Bi, J., Mendes de Moura, Y., and Sellers, P. J.: Vegetation dynamics and rainfall sensitivity of the Amazon, Proceedings of the National Academy of Sciences, 111, 16 041–16 046, 2014.

Hogan, J. A., Domke, G. M., Zhu, K., Johnson, D. J., and Lichstein, J. W.: Climate change determines the sign of productivity trends in US forests, Proceedings of the National Academy of Sciences, 121, e2311132 121, 2024.

Hubau, W., Lewis, S. L., Phillips, O. L., Affum-Baffoe, K., Beeckman, H., Cuní-Sanchez, A., Daniels, A. K., Ewango, C. E., Fauset, S., Mukinzi, J. M., et al.: Asynchronous carbon sink saturation in African and Amazonian tropical forests, Nature, 579, 80–87, 2020.

Janssen, T., Fleischer, K., Luyssaert, S., Naudts, K., and Dolman, H.: Drought resistance increases from the individual to the ecosystem level in highly diverse Neotropical rainforest: a meta-analysis of leaf, tree and ecosystem responses to drought, Biogeosciences, 17, 2621–2645, 2020.

Jiménez-Muñoz, J. C., Mattar, C., Barichivich, J., Santamaría-Artigas, A., Takahashi, K., Malhi, Y., Sobrino, J. A., and Schrier, G. v. d.: Record-breaking warming and extreme drought in the Amazon rainforest during the course of El Niño 2015–2016, Scientific reports, 6, 33 130, 2016.

Koch, A. and Kaplan, J. O.: Tropical forest restoration under future climate change, Nature Climate Change, 12, 279–283, 2022.

Koven, C. D., Knox, R. G., Fisher, R. A., Chambers, J. Q., Christoffersen, B. O., Davies, S. J., Detto, M., Dietze, M. C., Faybishenko, B., Holm, J., et al.: Benchmarking and parameter sensitivity of physiological and vegetation dynamics using the Functionally Assembled Terrestrial Ecosystem Simulator (FATES) at Barro Colorado Island, Panama, Biogeosciences, 17, 3017–3044, 2020.

Lin, S., Chen, X., Xia, J., Xin, Q., Fu, Z., He, B., Liu, Q., Piao, S., and Yuan, W.: Global vegetation production may decrease in this century due to rising atmospheric dryness, Nature Ecology & Evolution, pp. 1–11, 2025.

Longo, M., Knox, R. G., Levine, N. M., Alves, L. F., Bonal, D., Camargo, P. B., Fitzjarrald, D. R., Hayek, M. N., Restrepo-Coupe, N., Saleska, S. R., et al.: Ecosystem heterogeneity and diversity mitigate Amazon forest resilience to frequent extreme droughts, New Phytologist, 219, 914–931, 2018.

Malhi, Y.: The carbon balance of tropical forest regions, 1990–2005, Current Opinion in Environmental Sustainability, 2, 237–244, 2010.

Maréchaux, I., Fischer, F. J., Schmitt, S., and Chave, J.: TROLL 4.0: representing water and carbon fluxes, leaf phenology, and intraspecific trait variation in a mixed-species individual-based forest dynamics model – Part 1: Model description, Geoscientific Model Development, 18, 5143–5204, https://doi.org/10.5194/gmd-18-5143-2025, 2025.

Martínez Cano, I., Shevliakova, E., Malyshev, S., Wright, S. J., Detto, M., Pacala, S. W., and Muller-Landau, H. C.: Allometric constraints and competition enable the simulation of size structure and carbon fluxes in a dynamic vegetation model of tropical forests (LM3PPA-TV), Global Change Biology, 26, 4478–4494, 2020.

Nakad, M., Sevanto, S., Domec, J.-C., and Katul, G.: Linking the Water and Carbon Economies of Plants in a Drying and Warming Climate, Current Forestry Reports, 9, 383–400, 2023.

Nepstad, D., Moutinho, P., Dias-Filho, M., Davidson, E., Cardinot, G., Markewitz, D., Figueiredo, R., Vianna, N., Chambers, J., Ray, D., et al.: The effects of partial throughfall exclusion on canopy processes, aboveground production, and biogeochemistry of an Amazon forest, Journal of Geophysical Research: Atmospheres, 107, LBA–53, 2002.

Pan, Y., Birdsey, R. A., Phillips, O. L., Houghton, R. A., Fang, J., Kauppi, P. E., Keith, H., Kurz, W. A., Ito, A., Lewis, S. L., et al.: The enduring world forest carbon sink, Nature, 631, 563–569, 2024.

Parsons, L. A.: Implications of CMIP6 projected drying trends for 21st century Amazonian drought risk, Earth's Future, 8, e2020EF001 608, 2020.

https://doi.org/10.5194/egusphere-2026-145
Preprint. Discussion started: 5 February 2026

Rice, A. H., Pyle, E. H., Saleska, S. R., Hutyra, L., Palace, M., Keller, M., de Camargo, P. B., Portilho, K., Marques, D. F., and Wofsy, S. C.: Carbon balance and vegetation dynamics in an old-growth Amazonian forest, Ecological applications, 14, 55–71, 2004.

Robbins, Z., Chambers, J., Chitra-Tarak, R., Christoffersen, B., Dickman, L. T., Fisher, R., Jonko, A., Knox, R., Koven, C., Kueppers, L., et al.: Future climate doubles the risk of hydraulic failure in a wet tropical forest, New Phytologist, 244, 2239–2250, 2024.

Rowland, L., da Costa, A. C. L., Galbraith, D. R., Oliveira, R. S., Binks, O. J., Oliveira, A. A., Pullen, A., Doughty, C. E., Metcalfe, D., Vasconcelos, S. S., et al.: Death from drought in tropical forests is triggered by hydraulics not carbon starvation, Nature, 528, 119–122, 2015.

Schmitt, S., Fischer, F. J., Ball, J. G. C., Barbier, N., Boisseaux, M., Bonal, D., Burban, B., Chen, X., Derroire, G., Lichstein, J. W., Nemetschek, D., Restrepo-Coupe, N., Saleska, S., Sellan, G., Verley, P., Vincent, G., Ziegler, C., Chave, J., and Maréchaux, I.: TROLL 4.0: representing water and carbon fluxes, leaf phenology, and intraspecific trait variation in a mixed-species individual-based forest dynamics model – Part 2: Model evaluation for two Amazonian sites, Geoscientific Model Development, 18, 5205–5243, https://doi.org/10.5194/gmd-18-5205-2025, 2025.

Seneviratne, S. I., Zhang, X., Adnan, M., Badi, W., Dereczynski, C., Di Luca, A., Gami, A. S., Iskandar, S., Kossin, J., Lewis, S., Otto, F., Pinto, I., Satoh, M., Vicente-Serrano, S. M., Wehner, M., and Zhou, B.: Weather and Climate Extreme Events in a Changing Climate, in: Climate Change 2021: The Physical Science Basis. Contribution of Working Group I to the Sixth Assessment Report of the Intergovernmental Panel on Climate Change, edited by Masson-Delmotte, V., Zhai, P., Pirani, A., Connors, S., Péan, C., Berger, S., Caud, N., Chen, Y., Goldfarb, L., Gomis, M., Huang, M., Leitzell, K., Lonnoy, E., Matthews, J., Maycock, T., Waterfield, T., Yelekçi, O., Yu, R., and Zhou, B., Cambridge University Press, https://doi.org/10.1017/9781009157896.013, 2021.

Shevliakova, E., Malyshev, S., Martinez-Cano, I., Milly, P., Pacala, S., Ginoux, P., Dunne, K., Dunne, J., Dupuis, C., Findell, K., et al.: The land component LM4. 1 of the GFDL Earth System Model ESM4. 1: Model description and characteristics of land surface climate and carbon cycling in the historical simulation, Journal of Advances in Modeling Earth Systems, 16, e2023MS003 922, 2024.

Strigul, N., Pristinski, D., Purves, D., Dushoff, J., and Pacala, S.: SCALING FROM TREES TO FORESTS: TRACTABLE MACROSCOPIC EQUATIONS FOR FOREST DYNAMICS, Ecological Monographs, 78, 523–545, https://doi.org/https://doi.org/10.1890/08-0082.1, 2008.

Sullivan, M. K., Fayolle, A., Bush, E., Ofosu-Bamfo, B., Vleminckx, J., Metz, M. R., and Queenborough, S. A.: Cascading effects of climate change: new advances in drivers and shifts of tropical reproductive phenology, Plant Ecology, 225, 175–187, 2024.

Tschumi, E., Lienert, S., van der Wiel, K., Joos, F., and Zscheischler, J.: The effects of varying drought-heat signatures on terrestrial carbon dynamics and vegetation composition, Biogeosciences, 19, 1979–1993, https://doi.org/10.5194/bg-19-1979-2022, 2022.

Ukkola, A. M., De Kauwe, M. G., Roderick, M. L., Abramowitz, G., and Pitman, A. J.: Robust future changes in meteorological drought in CMIP6 projections despite uncertainty in precipitation, Geophysical Research Letters, 47, e2020GL087 820, 2020.

Von Buttlar, J., Zscheischler, J., Rammig, A., Sippel, S., Reichstein, M., Knohl, A., Jung, M., Menzer, O., Arain, M. A., Buchmann, N., et al.: Impacts of droughts and extreme-temperature events on gross primary production and ecosystem respiration: a systematic assessment across ecosystems and climate zones, Biogeosciences, 15, 1293–1318, 2018.

Weng, E., Dybzinski, R., Farrior, C. E., and Pacala, S. W.: Competition alters predicted forest carbon cycle responses to nitrogen availability and elevated CO 2: simulations using an explicitly competitive, game-theoretic vegetation demographic model, Biogeosciences, 16, 4577–4599, 2019.

Weng, E., Aleinov, I., Singh, R., Puma, M. J., McDermid, S. S., Kiang, N. Y., Kelley, M., Wilcox, K., Dybzinski, R., Farrior, C. E., Pacala, S. W., and Cook, B. I.: Modeling demographic-driven vegetation dynamics and ecosystem biogeochemical cycling in NASA GISS's Earth

https://doi.org/10.5194/egusphere-2026-145
Preprint. Discussion started: 5 February 2026

system model (ModelE-BiomeE v.1.0), Geoscientific Model Development, 15, 8153–8180, https://doi.org/10.5194/gmd-15-8153-2022, 2022.

Weng, E. S., Malyshev, S., Lichstein, J. W., Farrior, C. E., Dybzinski, R., Zhang, T., Shevliakova, E., and Pacala, S. W.: Scaling from individual trees to forests in an Earth system modeling framework using a mathematically tractable model of height-structured competition, Biogeosciences, 12, 2655–2694, https://doi.org/10.5194/bg-12-2655-2015, 2015.

Windsor, D. M.: Climate and moisture variability in a tropical forest: long-term records from Barro Colorado Island, Panama, Smithsonian contributions to the earth sciences, 1990.

Xu, M., Bravo de Guenni, L., and Córdova, J. R.: Climate change impacts on rainfall intensity–duration–frequency curves in local scale catchments, Environmental Monitoring and Assessment, 196, 372, 2024.

Xu, X., Medvigy, D., Powers, J. S., Becknell, J. M., and Guan, K.: Diversity in plant hydraulic traits explains seasonal and inter-annual variations of vegetation dynamics in seasonally dry tropical forests, New Phytologist, 212, 80–95, 2016.